Research Article

Yuxuan Zhang, Shi Yan*, Lili Jiang*, Tiancong Fan, Junjun Zhai, and Hanhua Li

Couple effects of multi-impact damage and CAI capability on NCF composites

https://doi.org/10.1515/rams-2024-0003 received October 02, 2023; accepted March 01, 2024

Abstract: In this study, the mechanical properties of noncrimp fabric (NCF) composite laminates under low-velocity impact and compression after impact (CAI) tests were studied by Scanning electron microscopy (SEM) and Digital image correlation (DIC) techniques. The impact response under different impact times, impact angles, and impact distance is studied. Similarly, in CAI test, DIC technique is used to reveal the whole process of NCF composite compression failure, and SEM is used to reveal the microscopic failure form. The experimental results show that the impact damage process of NCF composites has strong directivity. The concrete manifestation is that the internal failure will extend along the paving direction at the failure layer. The peak load generated under 20 J impact energy is about 1/2 of that under 40 J impact energy. The impact distance is one of the important factors affecting the coupling effect of multiple impacts, and the impact angle has little effect on the internal damage extension. The proportion of internal damage area also supports the relevant view, that is, the average difference in the proportion of internal damage area under different impact distance is about 5%, while the average difference in the proportion of internal damage area under different impact angles is about 3%. During the compression process, the main failure mode is shear failure and the failure mode is brittle fracture. The oblique fracture

occurs only when the oblique is 45° and the impact distance is large (50 mm). The impact angle has little effect on the residual compression performance of NCF.

Keywords: NCF, multi-impact, compression after impact, C-scan, DIC, SEM

1 Introduction

Due to its higher specific strength, specific stiffness, and other characteristics, composite materials are widely used in aerospace, automobile manufacturing, medical equipment, sports equipment, and other fields [1-3]. In advanced engineering applications, although 2D woven fabric reinforced composites have high mechanical properties in the in-plane direction, they are prone to delamination damage under external loads such as impact and bending. Noncrimp fabric (NFC) is a type of composite material consisting of layers of different orientated thread fibers connected together by means of braiding [4]. Laminate is a kind of composite material with multi-layer structure. The performance of the laminates is determined by the arrangement of each layer, the layering angle, and the number of layers. The manufacturing process of NCF composite material is shown in Figure 1. NCF composites are often affected by dynamic loads such as the impact during use. The impacts are generally divided into low-velocity impact and high-velocity impact. Low-velocity impact (LVI) often produces barely visible impact damage, in which the structure degenerates in various hidden failure mechanisms, such as fiber breakage, matrix cracking, kinking bands, and delamination [5]. Therefore, it is necessary to carry out impact tests on NCF composites. Similarly, after the impact, the compression experiment of the material will effectively measure its residual compression performance.

Although many scholars and institutions have made certain research on the mechanical properties of composite laminates, the research on LVI test and CAI test of NCF composites is still limited [6]. Atas *et al.* [7] studied the impact response of patched and unpatched glass/epoxy composite plates. Shyr and Pan [8] studied the damage

Yuxuan Zhang: Department of Engineering Mechanics, Harbin University of Science and Technology, Harbin, 150000, China Tiancong Fan: Aulin College, Northeast Forestry University Harbin, Harbin 150000, China

Junjun Zhai: College of Aeronautics and Astronautics, North China Institute of Aerospace Engineering, Langfang 065000, China **Hanhua Li:** Department of Engineering Mechanics, Beijing Institute of Astronautical Systems Engineering, Beijing 100076, China

^{*} Corresponding author: Shi Yan, Department of Engineering Mechanics, Harbin University of Science and Technology, Harbin, 150000, China, e-mail: yanshi@hrbust.edu.cn

^{*} Corresponding author: Lili Jiang, College of Civil Engineering and Architecture, Xiamen City University, Xiamen 361008, China, e-mail: 1458994695@qq.com

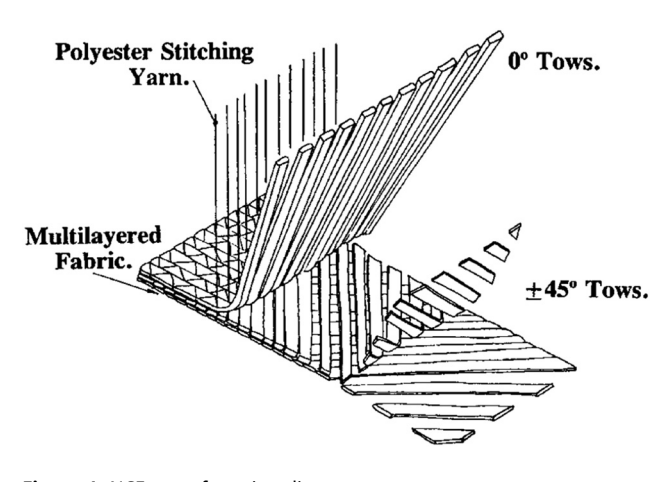


Figure 1: NCF manufacturing diagram.

characteristics and failure strength of composite laminates in low-speed impact tests. Shyr et al. [9] determined the impact damage and growth behavior of T700 multi-axial suture CFRP. Saito et al. [10] studied the effect of CF/GF fiber mixture on the impact properties of multi-axial warp-knitted fabric composites. Bouvet et al. [11] and Shi et al. [12] proposed a model to predict the permanent indentation caused by LVI and validate a single reference layup for a given impact energy. Hongkarnjanakul et al. [13] extended Bouvet's work by changing the impact conditions using different stacking sequences to verify the initial model, with a single impact energy value of 25 J. Other relevant studies have shown [14-21] that in terms of structural properties, thin fabric layer has higher destructive capacity than thick fabric layer. Meanwhile, García-Rodríguez et al. [3] used NCF composites to study the effect of fabric thickness on impact and CAI strength, and proved the sequence of failure. In addition, damage tolerance is defined as the ability to maintain undamaged or initial strength in the presence of damage. It is quantified by measuring the tensile after impact, compression after impact (CAI), and flexure after impact [22]. Compared to 2D or 3D braided composites (3DBC), NCF composites may have a higher CAI strength after a single impact due to the superior compressive strength despite larger lamination areas [23]. The failure mechanism under compression was originally studied by Argon [24] and it was determined that the initial fiber misalignment relative to the laminate and loading direction led to matrix shear failure, resulting in the formation of a kink band. Recently, Shipsha et al. [25] studied the compressive strength and damage mechanism of cross-ply NCF composites at different off-axis angles and determined that the main failure mechanism for all samples was fiber kink.

Based on the existing literature, the whole process of LVI and CAI testing of NCF composites is still lacking in a variety of technical means. Though, in numerical simulation, many models, more experimental damage criteria, smaller representative volume element, etc., have been established. However, in terms of experiments, observations and statistics are still carried out in a single way. It is not conducive to propose more detailed damage mechanism and more effective damage criteria. The purpose of LVI experiment on experimental materials is to study the influence of structural damage caused by accumulative minor damage of the internal fibers and matrix of NCF materials under multiple low-speed impacts. This has an important impact on the actual service cycle of NCF materials, and also has a certain guiding significance for the impact resistance design of materials. At the same time, CAI experiment is an effective way to study and predict the damage growth dynamics of NCF composites. Through CAI experiments, it is helpful to study the damage evolution process of materials, and also help to propose more accurate damage models [26,27]. Therefore, this experiment innovatively combines the use of Digital image correlation (DIC) with Scanning electron microscopy (SEM) to test LVI and CAI on specimens. The failure process was observed and the damage was assessed. At the same time, there are few studies on multiple shock effects at different spacings in the existing literatures. Therefore, further experimental analysis is carried out for multiple impact damage and residual compression properties. This research not only has a certain guiding significance for engineering practice, but also has a certain significance for improving numerical simulation.

2 Materials and process

2.1 Materials and equipment

The carbon fiber model of NCF composite material selected in this test is domestic CCF3003k (Toray T3003k carbon fiber). Fabric layer structure of 0/+45/90/-45, laminated layer of galley way for $[0^\circ/+45^\circ/90^\circ/-45^\circ, +45^\circ/90^\circ/-45^\circ]_{2s}$, and related parameters are shown in Table 1.

The size of NCF composite material selected for the test was $100 \text{ mm} \times 150 \text{ mm} \times 5 \text{ mm}$, and the actual measurement error was $\pm 0.5 \text{ mm}$. Figure 2 shows the upper and lower surfaces and sides of the NCF composite used in the test.

Table 1: Material parameters

Fiber type	Tensile strength (MPa)	E (GPa)	Elongation after breaking (%)	Density (g·cm ^{−3})
CCF300 3k	3,900	220	1.86	1.78

2.2 LVI

The main experimental instruments used in LVI testing are drop hammer impact testing machines, custom fixtures, spherical punches, and C-scan (for non-destructive testing, NDT).

The LVI test process is as follows: install the specimen horizontally in the pneumatic clamp for positioning and fixing, adjust the impact point position, set the impact energy and other parameters, and start the experiment after the adjustment. The equipment name and model parameters are shown in Table 2 and Figure 3.

The working principle of the drop hammer impact testing machine is based on the kinetic energy theorem. By setting the required energy (20, 30, or 40 J) in the Instron-9250HV system, the system will automatically match the required hammer height according to the total mass of the punch system so as to ensure the energy required for impact. It is worth noting

Table 2: Name and model of the impact test equipment

Model	Main parameter	
Instron-9250HV	Maximum impact energy: 826 J Maximum impact velocity: 20 m·s ⁻¹ Punch positioning accuracy: 0.1 mm	

that the top of the testing machine is also provided with a spring when higher impact energy is required. Through the compression of the spring, the elastic potential energy is further converted into impact energy. Since the main test environment for this test is low-speed impact, this process is not required. In the test, the testing machine can automatically collect the data of punch energy, speed, displacement, failure load, failure displacement, failure energy, etc., which provide the data basis for subsequent analysis. The total quality of the punch system is shown in Table 3.







Figure 2: NCF composite specimens. (a) Specimen upper surface (impact surface), (b) lower surface of specimen, and (c) specimen side.

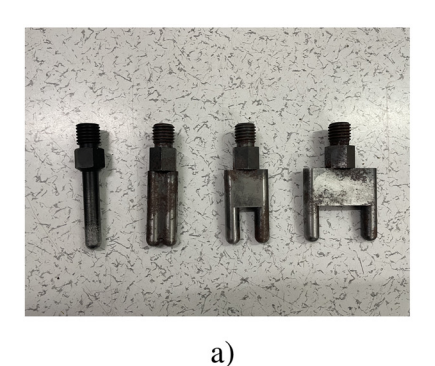






Figure 3: Impact test equipment. (a) Punch, (b) drop hammer impact testing machines, and (c) C-scan.

Table 3: Total mass of punch system

Punch type	<i>m</i> (kg)
Single head ball punch	7.29 kg
12.5 mm pitch double head ball punch	7.36 kg
25 mm pitch double head ball punch	7.40 kg
50 mm pitch double head ball punch	8.20 kg

Table 4: Impact test group and specimen number

Experimen- tal group	LVI-test angle/ energy	/ Spe	Specimen number		
		12.5 mm	25 mm	50 mm	
Group 1	Angles 1	12.5-20J-1	25-20J-1	50-20J-1	
·	J	12.5-40J-1	25-40J-1	50-40J-1	
	Angles 2	12.5-20J-2	25-20J-2	50-20J-2	
	J	12.5-40J-2	25-40J-2	50-40J-2	
	Angles 3	12.5-20J-3	25-20J-3	50-20]-3	
	J	12.5-40J-3	25-40J-3	50-40J-3	
	Angles 4	12.5-20J-4	25-20J-4	50-20J-4	
	J	12.5-40J-4	25-40J-4	50-40J-4	
Group 2	20 J	12.5-20J-1	25-20J-1	50-20J-1	
		12.5-20J-2	25-20J-2	50-20J-2	
		12.5-20J-3	25-20J-3	50-20J-3	
		12.5-20J-4	25-20J-4	50-20J-4	
	40 J	12.5-40J-1	25-40J-1	50-40J-1	
		12.5-40J-2	25-40J-2	50-40J-2	
		12.5-40J-3	25-40J-3	50-40J-3	
		12.5-40J-4	25-40J-4	50-40J-4	
			Geomet	ric center	
Control group)	20 J	20J-1		
- '		30 J	30J-1		
		40 J	40J-1		

The specific groups of LVI experiments are as follows. The specific specimen numbers and groups are shown in Table 4.

- 1) Group 1: Influence of different shock times at the same distance and angle;
- 2) Group 2: The influence of different impact angles at the same distance and energy;
- 3) Control group: The impact energy of 20, 30, and 40 J was set for the experiment.

Test parts are labelled in the way of "impact distance – impact energy – angle type." For example, 12.5 mm to 20 J-1 indicates low-speed impact at 12.5 mm impact distance, with 20 J impact energy and impact position in the direction of Angle 1. Different from groups 1 and 2, the impact position of the control group is at the geometric center. Except for the control group, there are four kinds of impact angle positions, as shown in Figure 4.

2.3 CAI

The CAI test was carried out using an electronic universal testing machine, and the compression failure process was monitored by DIC. The equipment names and parameters required for specific experiments are shown in Table 5.

The axial compression test was carried out by electronic universal testing machine. The part of the testing machine is composed of two pressure plates up and down and four fixed fixtures, the lower pressure plate is used to undertake the experimental fixture, and the upper pressure plate is used to load the specimen at a constant speed. The

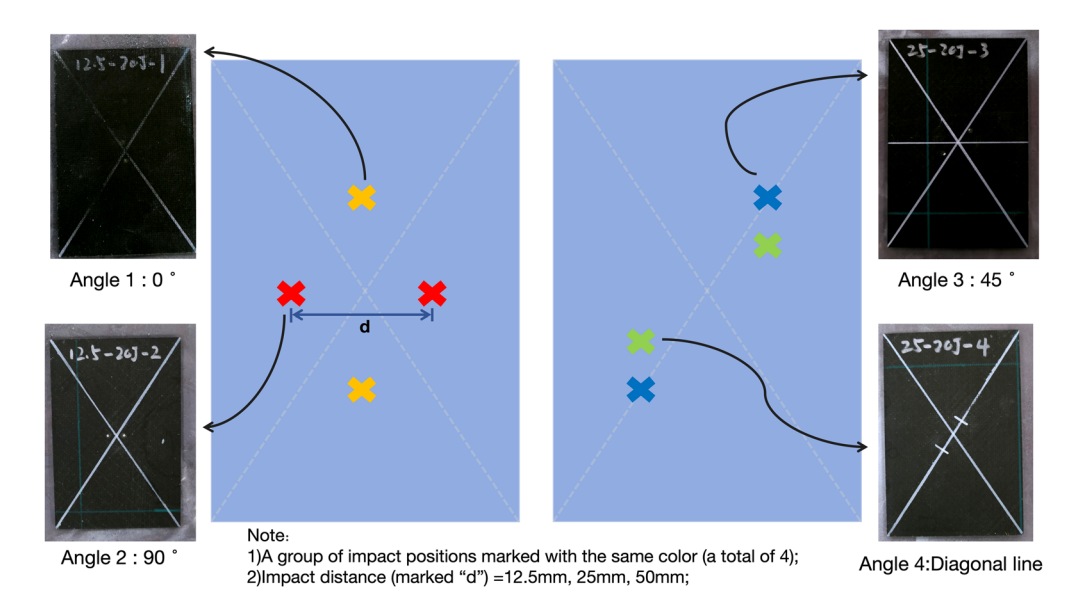


Figure 4: Description of impact angle category.

Table 5: Name and model of the compression test equipment

Model	Main parameter
WDW-200	Maximum loading: 200 kN Test force resolution: 1/500,000 Minimum read value of deformation: 0.01 mm Repeatability relative error of test force indication value ≤1% Test force zero relative error: ±0.1% Loading speed range: 0.05–500 mm·min ⁻¹

maximum experimental load is 200 kN, and the testing machine has an overload protection mechanism, that is, when the maximum experimental load is exceeded, the alarm is automatically generated and the loading is stopped.

During the experiment, the specimen was first jammed, the four sides were completely fixed, and the vertical of the specimen was kept. The specimen was placed on the lower pressure plate, the loading speed was set at $0.5\,\mathrm{mm\cdot min^{-1}}$, and the experiment was compressed until the specimen was completely destroyed. The experimental equipment is shown in Figure 5. At the same time, DIC technology is used to monitor the whole process of compression.

2.4 NDT process

2.4.1 C-scan

In this experiment, C-scan was used to detect the internal damage area of the specimen. Since the emission direction of the ultrasonic wave in C-scan is perpendicular to the

Table 6: Name and model of the C-scan

Model Main parameter	
Sonoscan-D9500	Probe frequency: 5–400 MHz Sound width: 0.25 ns to 1 µm Maximum scanning area: 333 mm × 312 mm X/Y-axis accuracy: ±0.5 µm Z-axis accuracy: ±45 nm

scanning plane, the image obtained after scanning is the superimposed area of the specimen being scanned. Table 6 shows the equipment parameters used in this test.

C-scan in this experiment consists of "pre-test part stage," "internal damage detection stage after LVI experiment" and "internal damage detection stage after CAI experiment." Through the above process, the shape of the damaged area, the direction of damage expansion, and the proportion of the damaged area inside the tested part are recorded, which provides data support for further damage mode analysis.

2.4.2 SEM

SEM enables the characterization and observation of organic and inorganic materials on the nanometer to micron (µm) scale. SEM supports high magnifications up to 300,000× and even 1,000,000×. The SEM equipment used in this experiment was SU5000 produced by Hitachi (Japan), and equipped with energy dispersive X-ray spectroscopy (EDS) function. The test process and equipment are shown in Figure 6.



a)



b)



c)

Figure 5: Universal testing machine and special fixture for compression test. (a) Electronic universal testing machine, (b) CAI test procedure, and (c) specimen loading fixture.

2.4.3 DIC

DIC is a kind of measurement technology based on optical measurement methods. Its basic principle is to divide the area of the tested object at pixel level through digital photography technology. After the surface speckle treatment of the test specimen in advance, the linear motion of the speckle is monitored. By recording this offset, the shape variable of the test area can be obtained. Reliable real-time damage monitoring technology is very important for monitoring the structural integrity, global displacement field, and global stress analysis of 2D laminates and 3DBC. DIC is particularly meaningful when the structure is subject to invisible damage that can lead to complete destruction. The experimental equipment parameters are shown in Table 7. The experimental process and specimen treatment are shown in Figure 7.

3 LVI test and experimental results

3.1 Analysis of impact behavior response

In general, the load–time curve obtained by the two different impact energies of 20 and 40 J presents four stages as a whole: an upward stage of approximately linear development – a stratification phenomenon leads to an inflection point – the contact force continues to rise to the peak load – and the strength of the specimen further decreases. Peak load refers to the maximum load generated by the impact, which indicates the maximum contact force received by the test part during the entire impact process. The first inflection point is the delamination threshold load (DTL). Under DTL load, the internal layer of the specimen appears for the first time, resulting in a sudden decline in the contact

(a)

Figure 6: (a) SEM test piece and (b) SEM equipment.

Table 7: Name and model of the C-scan

Model	Main parameter
VIC-3DSR	Camera resolution: 1,920 × 1,200 Frame rate: 140 Hz In-plane resolution: 0.000005 × FOV Out-of-plane displacement resolution: 0.00001 × FOV Strain resolution: minimum 10 με Strain range: 0.005 ≥ 2.000%

force. It should be noted that due to the difference in damage depth and damage region caused by different impact energies, DTL is different under different impact energies. Since the remaining unbroken structure will continue to provide structural strength, the contact force will continue to increase after a brief reduction until it reaches a peak load and begins to decrease

Figure 8 shows the load-time curve of the specimen under 20 J multiple impact test and 40 J single impact test. As can be seen from the figure, the peak load generated under 40 I impact test is nearly twice that generated under 20 J impact test. It should be noted that the time-load curve of 50-20J-2-2 shows obvious differences, showing a certain energy absorption effect and damage evolution. The reason for this phenomenon may be that the hygrothermal environment will increase the interlayer bonding force of the laminates, and then reduce the peak contact load under the impact [28]. Therefore, possible moisture exposure during specimen storage is the most important possible factor for the reduction in peak contact load. Similarly, the reduction in peak contact load due to the manufacturing defects of the specimen and the improper fixation of the specimen process is also the cause of this phenomenon.

Two different groups are analyzed in detail. The loadtime of group 1 (different shock times) is shown in Figure 9.







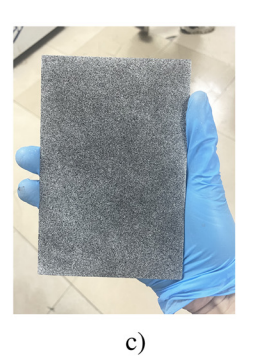


Figure 7: DIC and pretreatment of test pieces. (a) DIC monitoring process, (b) specimen surface pretreatment process, and (c) pretreated specimen.

1) Under multiple impact experiments conducted at 20 J impact energy.

The peak load generated by the second impact is slightly lower than that generated by the first impact. This shows that the first impact of the specimen leads to the internal damage of laminates such as delamination and spalling, which leads to the reduction in its strength. Thus, it can also be shown that the increase in the number of shocks will reduce the strength of the material. However, whether this trend will stabilize with the further increase in the number of shocks still needs to be supplemented with further multiple impact specimens. Similar trends are obtained under the four angles. Therefore, it can be considered that different impact angles have little influence on the peak load.

To be specific, at the distance of 12.5 mm, because the damage area generated by the first impact is larger than 12.5 mm, the impact point is in the first damage area when the second impact test is carried out. This is the reason why there is no inflection point (that is, DTL) in the load–time curve generated at the second impact at a distance of 12.5 mm. However, at 25 and 50 mm impact distance, due

to the large impact distance, the coupling impact effect of the impact experiment is not obvious, and the independence of the two impact experiments is stronger. Therefore, the load—time curves of the two shocks almost coincide, and the inflection point (DTL) occurs in the rising stage.

2) Under a single impact experiment at 40 J impact energy.

On the whole, it shows the same rule as 20 J multiple impact test. The load–time curve is consistent, the inflection point appears, and the peak load generation time is almost the same. Therefore, it can be considered that the impact response at 20 and 40 J impact energies is almost the same. Specifically, the peak load and DTL under a single impact of 40 J is nearly twice that under two impacts of 20 J.

The load-time of group 2 (different impact angles) is shown in Figure 10.

Since the number of shocks in 20 J is two times, to simplify the analysis results, only the data after the second impact is selected from the load–time curve of 20 J impact energy. According to the curve, it can be seen that the time for the contact force of 20 and 40 J to increase from 0 N to

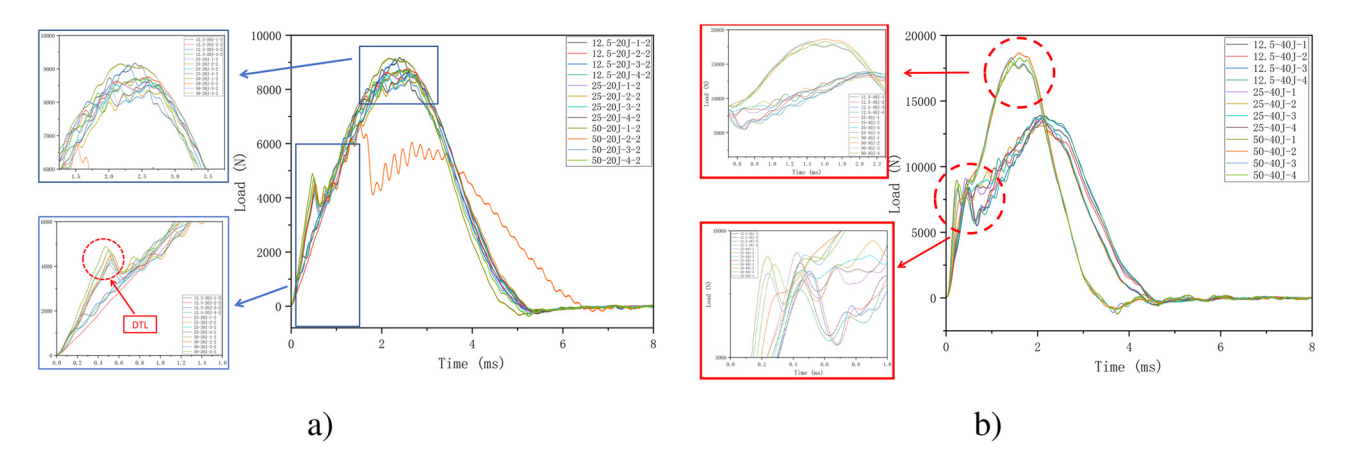


Figure 8: Load-time curves of specimens under (a) 20 J and (b) 40 J impact energy.

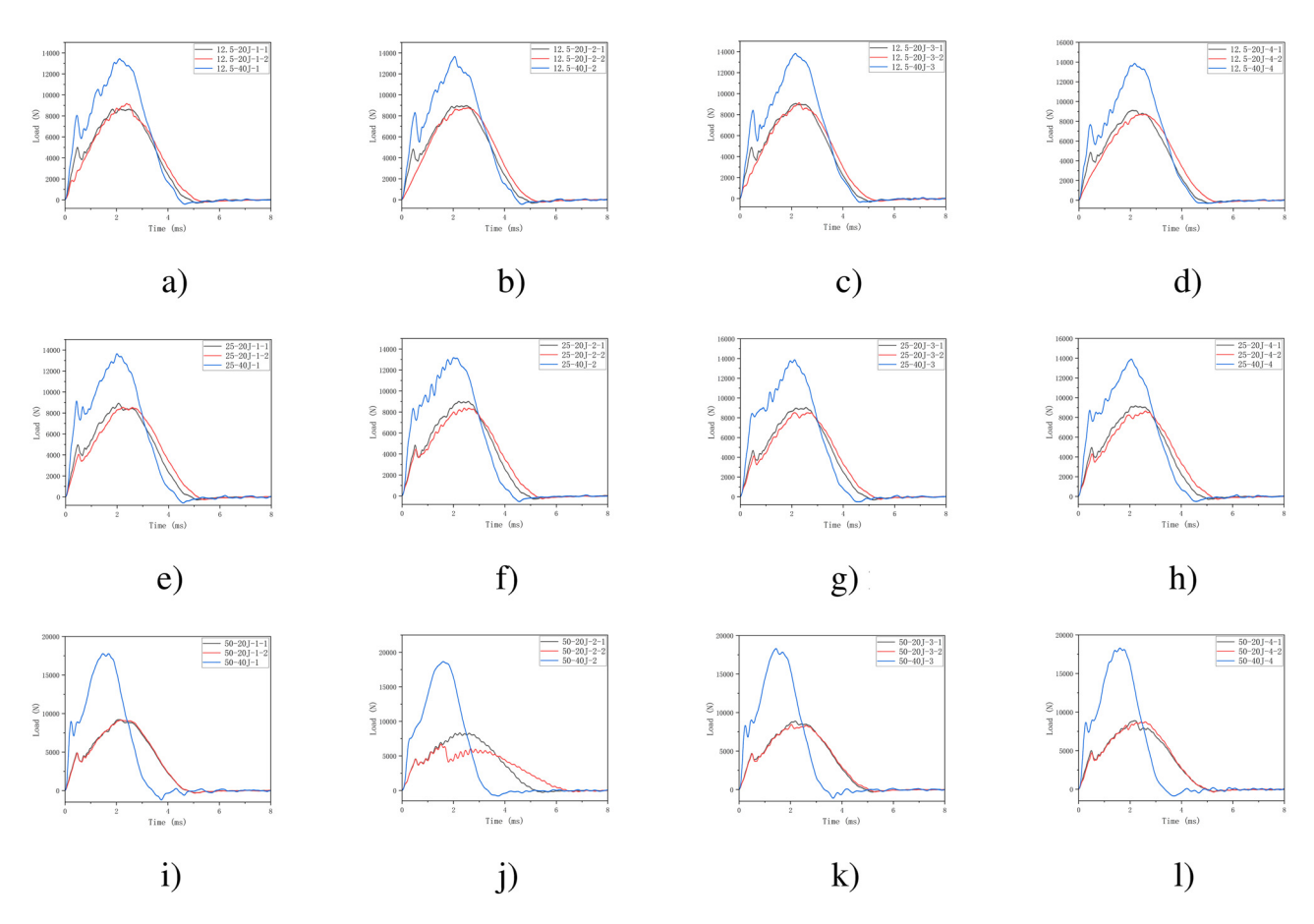


Figure 9: Load–time curve of grouped specimens under different impact times. (a) 12.5 mm⁻¹, (b) 12.5 mm⁻², (C) 12.5 mm⁻³, (d) 12.5 mm⁻⁴, (e) 25 mm⁻¹, (f) 25 mm⁻², (g) 25 mm⁻³, (h) 25 mm⁻⁴, (i) 50 mm⁻¹, (j) 50 mm⁻², (k) 50 mm⁻³, and (l) 50 mm⁻⁴.

the peak load is about 2 ms. However, under the impact energy force of 20 J, the peak load is about 4.5–5 ms after it returns to a stable state, and the distribution of 40 J is about 4.5 ms. This is because an increase in the number of shocks further leads to a decrease in strength compared to a single shock. As can be seen from the load–time curve in the same figure, the impact angle has little influence on the peak load, that is, the strength of the material.

3.2 Damage of impact analysis by C-scan

After passing the LVI test, the surface damage was observed first. The specimen was dented at the impact point, and the fibers in the dented region were mainly compressed and bent, but there were no obvious cracks and fiber fracture traces. At the lower surface of the specimen, the fiber bundle was broken along the 45° layup direction, and slight fault signs began to appear. Because the main factors affecting the strength of the laminates are the laying direction of each layer and the bonding of matrix between layers, there is a

certain directional shape of the failure crack. External characterization showed that the surface visible damage decreased with the increase in impact distance. This is due to the reduction in the impact coupling effect, resulting in internal damage independent of each other at the impact distance of 25 mm and 50 mm. After that, C-scan was performed on 20 J specimens. The C-scan results are shown in Figure 11, and the proportion of damaged areas is shown in Table 8. The overall results show that the impact damage area "expands with the impact point as the center of the circle and extends further along the direction of the damage layer."

Specifically, under the impact of 12.5 mm spacing, the second impact is affected by the first impact because the distance between the two impacts is relatively close. This influence is mainly reflected in the two impacts, and the support layer obtained at different angles is not the same, so the damage direction under the four impact angles does not have obvious regularity. At the same time, due to the coupling effect of two shocks, the damage area overlaps. This is also the main reason why the overall damage area

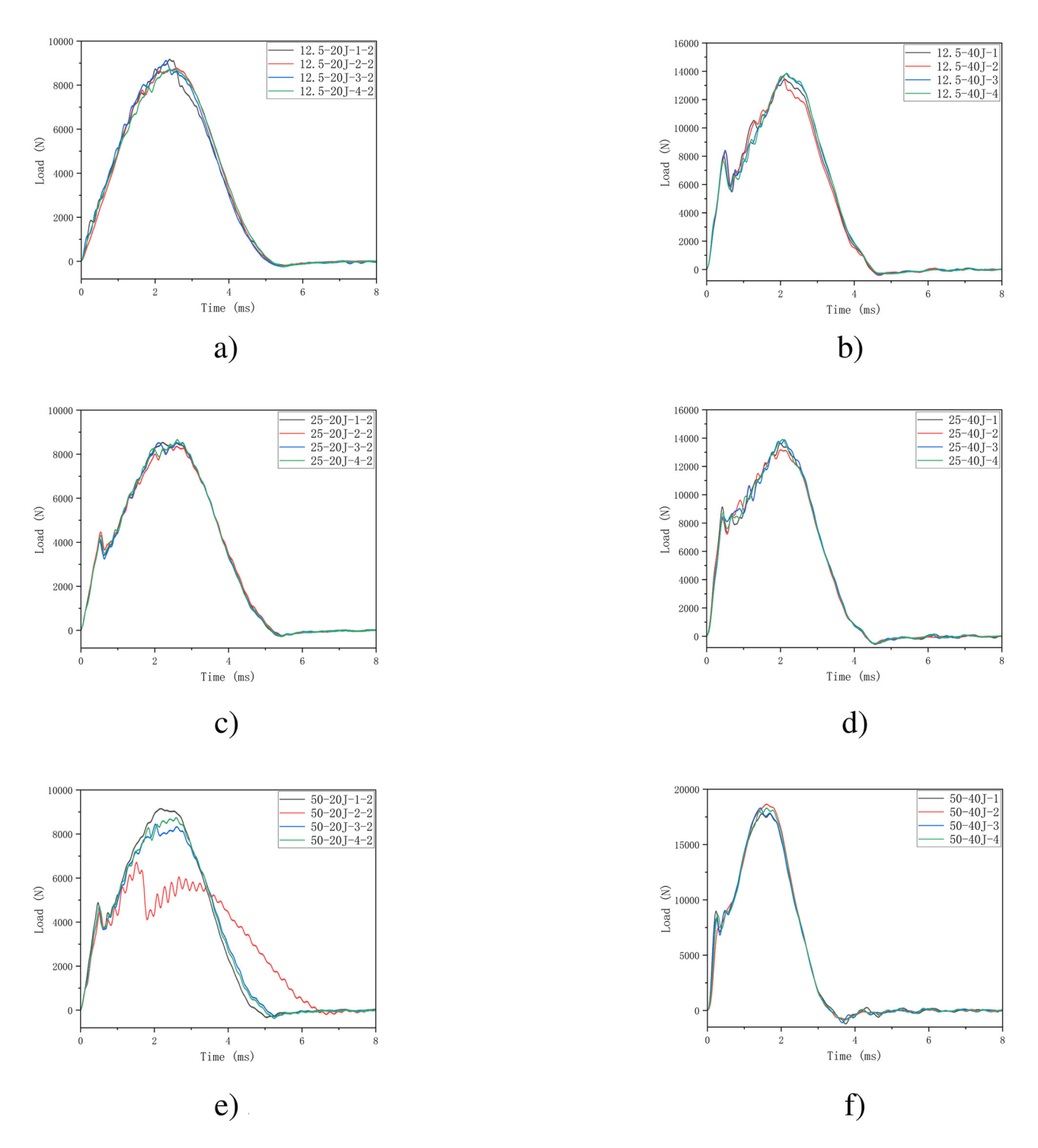


Figure 10: Load-time curves of grouped specimens under different impact angles. (a) 12.5 mm-20J, (b) 12.5 mm-40J, (c) 25 mm-20J, (d) 25 mm-40J, (e) 50 mm-20J, and (f) 50 mm-40J.

at 12.5 mm impact distance is larger than that at 25 mm spacing and 50 mm spacing. For multiple impact experiments at 25 and 50 mm spacing, the two impact experiments are approximately independent of each other due to the large impact distance. The observation results show

that the damage area, extension direction, and expansion form are almost the same under two impacts, respectively. Meanwhile, the damage development direction mainly develops along the fiber layering direction of the damage layer thickness, with strong directionality.

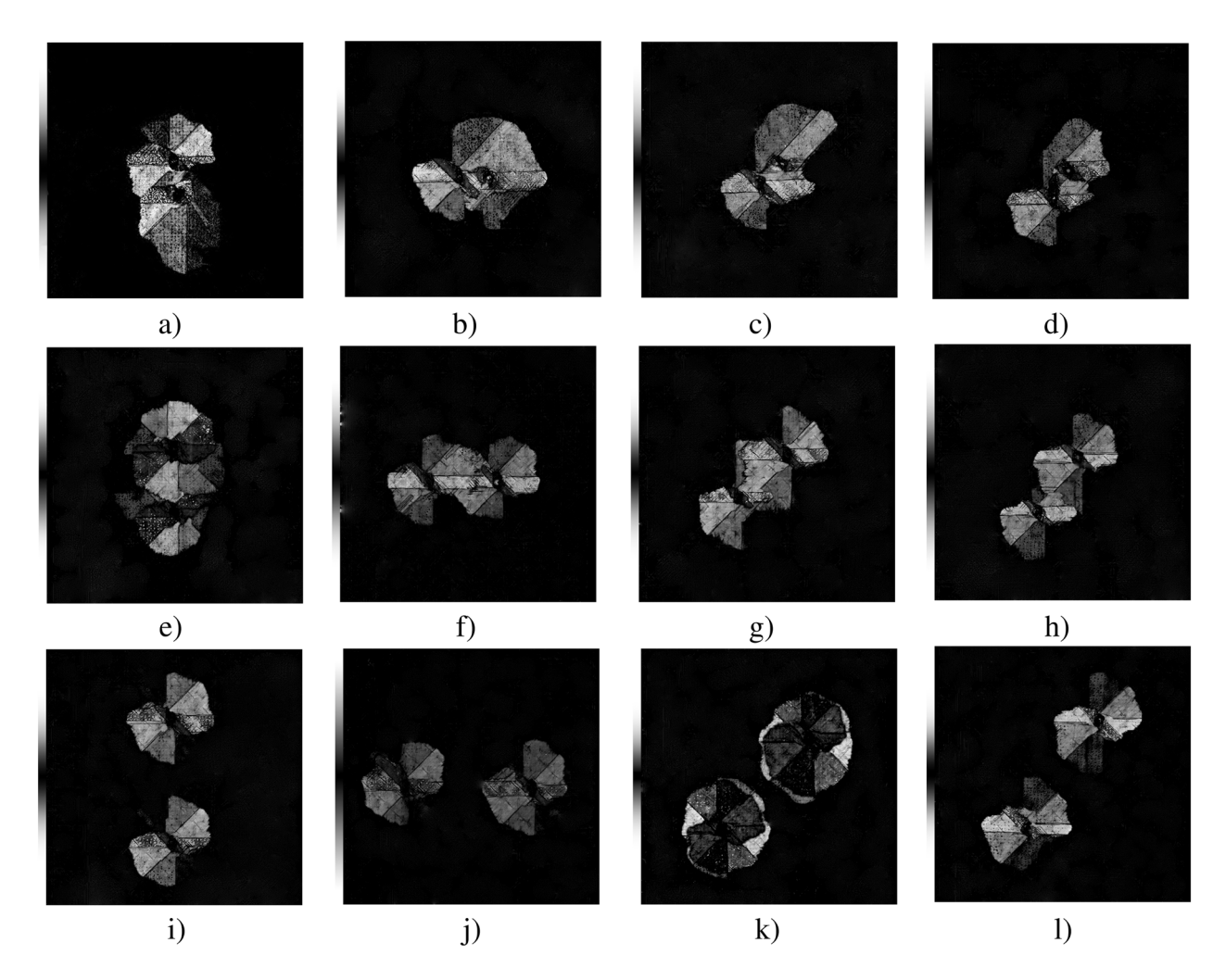


Figure 11: Internal damage of the specimen under 20 J impact. (a) 12.5 mm-20J-1, (b) 12.5 mm-20J-2, (C) 12.5 mm-20J-3, (d) 12.5 mm-20J-4, (e) 25 mm-20J-1, (f) 25 mm-20J-2, (g) 25 mm-20J-3, (h) 25 mm-20J-4, (i) 50 mm-20J-1, (j) 50 mm-20J-2, (k) 50 mm-20J-3, and (l) 50 mm-20J-4.

Table 8: Proportion of internal damage area under 20 J impact energy

Number	Proportion of damaged areas (%)	
12.5-20J-1	14.26	
12.5-20J-2	16.93	
12.5-20J-3	16.17	
12.5-20J-4	16.63	
25-20J-1	19.01	
25-20J-2	16.72	
25-20J-3	14.39	
25-20J-4	16.04	
50-20J-1	16.87	
50-20J-2	15.86	
50-20J-3	16.03	
50-20J-4	14.24	

After that, the 40 J specimen was C-scanned. The C-scan results are shown in Figure 12, and the proportion of

damaged areas is shown in Table 9. The overall results are consistent with the impact energy of 20 J.

Specifically, because it is a single double punch impact test, it will inevitably be affected by the horizontal accuracy of the pneumatic fixture, the height difference between the two points of the punch, the horizontal accuracy of the internal laying layer of the specimen, and other factors in the test. However, on the whole, the damage extension mode and direction are the same as the trend obtained under 20 J impact energy. According to the statistical results in Table 9, it can be found that the proportion of internal damage areas in 40 J is similar to that in 20 J. This shows that although the number of shocks increases, the strength decreases. However, since there is only one more test, whether this conclusion will show the same result with the further increase in the number of shocks, additional experiments are needed to prove it.

Finally, C-scan was performed on the control group. The C-scan results are shown in Figure 13, and the

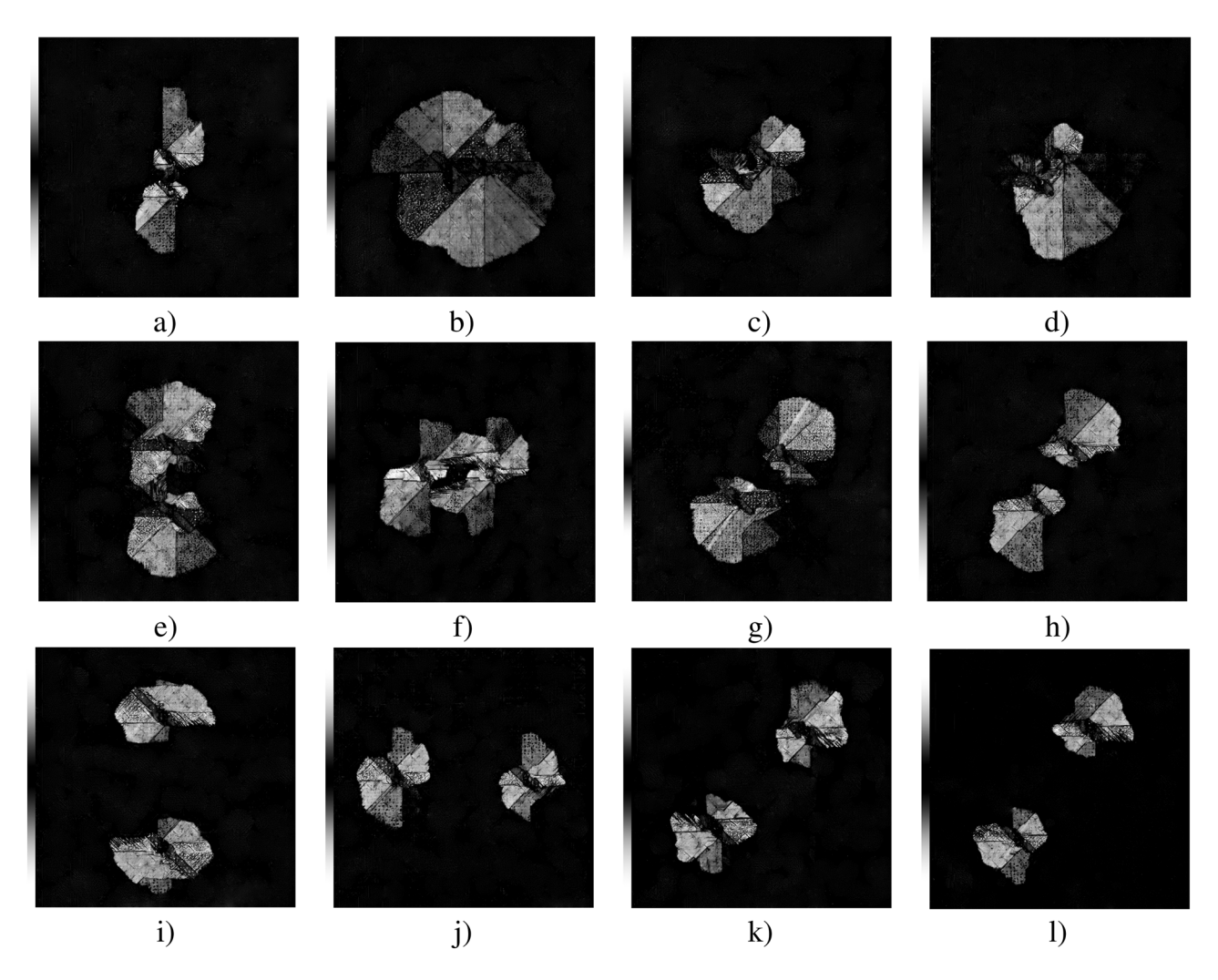


Figure 12: Internal damage of specimens under 40 J impact. (a) 12.5 mm-40J-1, (b) 12.5 mm-40J-2, (C) 12.5 mm-40J-3, (d) 12.5 mm-40J-4, (e) 25 mm-40J-1, (f) 25 mm-40J-2, (g) 25 mm-40J-3, (h) 25 mm-40J-4, (i) 50 mm-40J-1, (j) 50 mm-40J-2, (k) 50 mm-40J-3, and (l) 50 mm-40J-4.

Table 9: Proportion of internal damage area under 40 J impact energy

Number	Proportion of damaged areas (%)	
12.5-40J-1	13.82	
12.5-40J-2	17.95	
12.5-40J-3	15.95	
12.5-40J-4	16.44	
25-40J-1	16.21	
25-40J-2	18.29	
25-40J-3	15.86	
25-40J-4	17.01	
50-40J-1	14.03	
50-40J-2	12.04	
50-40J-3	15.29	
50-40J-4	14.36	

proportion of damaged areas is shown in Table 10. The conclusion of overall performance is the same. By calculating the

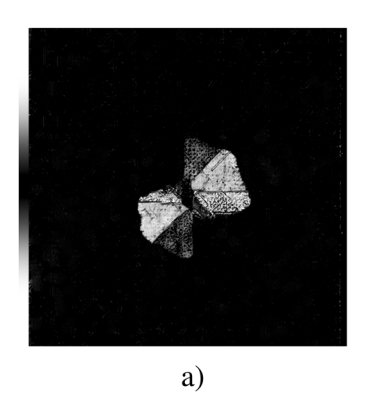
proportion of damage area, it can be found that the damage area increases with the increase in impact energy.

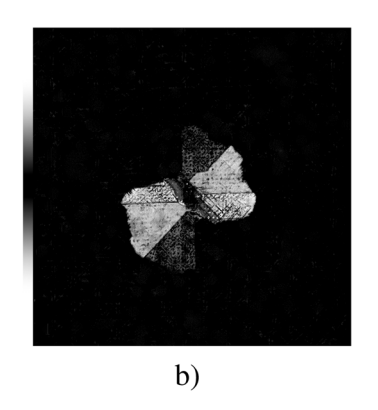
Specifically, because the control group is a single point of impact at the geometric center. Thus, the circular form of destruction is more obvious. According to the data in Table 10, it can be found that the damage area as a whole increases with the increase in impact energy.

4 CAI test and experimental results

4.1 Compression process analysis

By comparing the statistics of the ultimate load and the internal damage area during compression failure, the following conclusions can be drawn: The ultimate damage





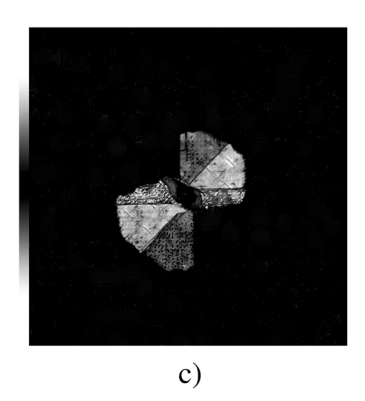


Figure 13: Internal damage of control group specimens. (a) 20J-1, (b) 30J-1, and (c) 40J-1.

Table 10: Proportion of internal injury area in the control group

Number	Proportion of damaged areas (%)
20J-1	8.09
30J-1	11.21
40J-1	12.31

load and the internal damage area show an overall trend of inverse proportion, that is, the greater the internal damage area, the lower the ultimate damage load. The specific statistics are shown in Figure 14. It should be noted that the damage area in Figure 14c is too large, which is inconsistent with the conclusion. The reason for this phenomenon may be caused by the inaccurate C-scan of the plate, or it may be caused by the manufacturing defect of the specimen.

The results of all specimens subjected to CAI tests were analyzed, and the "Displacement-Load" curve obtained according to the data is shown in Figures 15 and 16. All "displace-load" curves appear as a whole: "slow rise linear growth - peak Load after a sharp decline" three stages. The slow growth stage of the curve at the beginning of compression is caused by the false contact between the top of the specimen and the bottom of the pressure plate. Then, with the continuous increase in positive pressure, the compression stage begins. When the specimen reaches the ultimate load stage, the displacement and load value continue to maintain a linear increase trend. After the failure load is reached, brittle fracture occurs at the same time as the specimen, and the strength decreases sharply, and maintains a downward trend until the structural support is regained. During the experiment, the structure is brittle with loud fracture sound.

Specifically, first of all, for different shock times, with the increase in the number of shocks, the strength of the structure will decrease, but only one increase in the number of shocks has little effect on the strength decline. Therefore, there is little difference between the internal damage of the specimen under two impacts and that under a single impact, which is intuitively reflected in that the damage loads obtained by most curves are almost the same. Among some curves that produce peak load difference, most 20 J impact group produces lower damage load.

In the CAI test under different impact angles, the impact angle has little influence on the failure load. The reason for this is because the NCF composite material selected in this test is eight-layer composite board, in the impact test, the thickness of the failure layer is not uniform, so the failure direction is not uniform, resulting in this situation.

The displacement—load curve obtained from the experimental data of the control group is shown in Figure 16. The experimental results of control group show that the peak load decreases with the increase in impact energy. This is due to the increase in the internal damage area with the increase in the impact energy, resulting in a reduction in the strength of the material structure, so the peak load is reduced. The overall conclusion is the same as above.

4.2 Analysis of DIC monitoring damage evolution process

By monitoring the typical stages of compression damage of specimens 25-40J-3, the development form of failure can be seen. With the increase in vertical positive pressure, the impact point of punch and the damaged area of fiber are further subjected to vertical pressure and shear action, and the phenomenon of stress concentration occurs. The local stress increases further until the brittle fracture occurs when the failure load is reached. Cracks often penetrate the impact point and extend laterally until a penetrating fracture is formed. See Figure 17 for details, where "V" represents "vertical displacement," " E_{yy} " represents

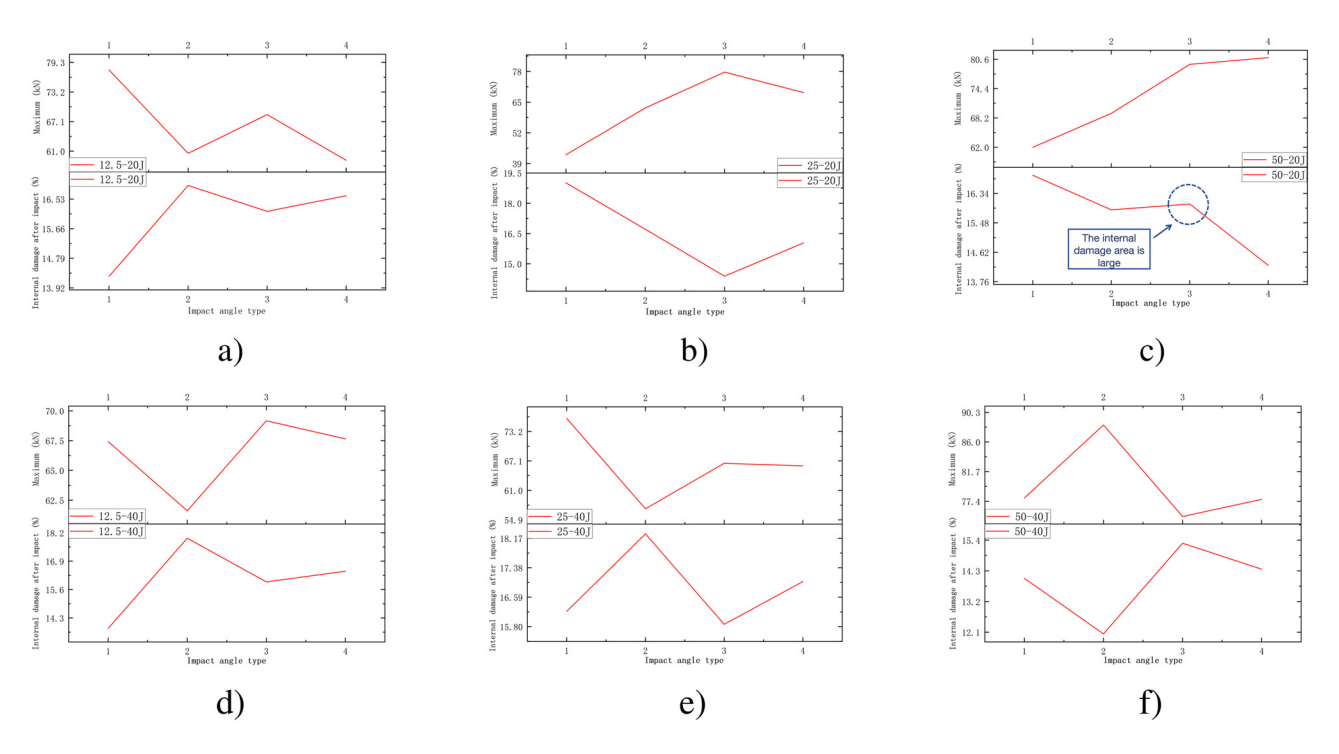


Figure 14: Comparison between maximum load and internal damage area. (a) 12.5-20J, (b) 25-20J, (c) 50-20J, (d) 12.5-40J, (e) 25-40J, and (f) 50-40J.

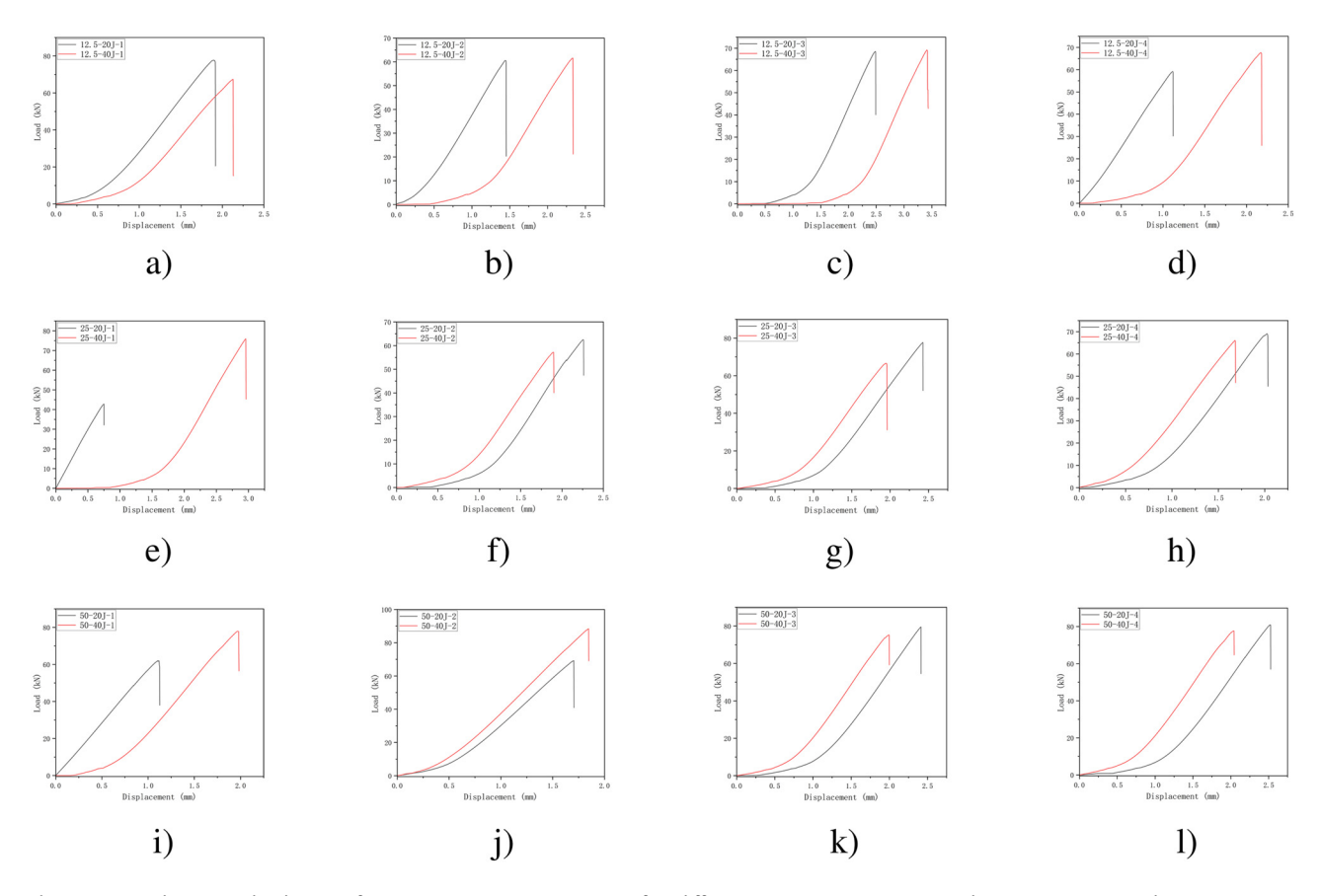


Figure 15: Displacement–load curves from compression experiments after different impact times. (a) 12.5-1, (b) 12.5-2, (c) 12.5-3, (d) 12.5-4, (e) 25-1, (f) 25-2, (g) 25-3, (h) 25-4, (i) 50-1, (j) 50-2, (k) 50-3, and (l) 50-4.

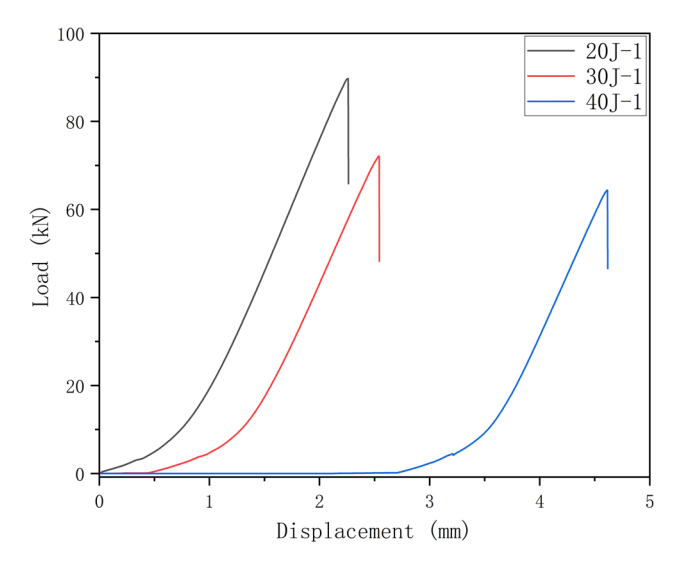


Figure 16: Displacement–load curve from compression experiment of control group specimens.

"vertical stress," and "*E*₂" represents the principal stress in the second direction.

The main recorded data "V" in the CAI test process, and the results of all its groups are shown in Figures 18-20. The results show that the form of compression failure is usually transverse fracture, and the impact angle has little effect on the fracture direction. The oblique fracture occurs only when the oblique fracture is 45° and the impact distance is large (50 mm). When compression failure occurs, the upper part is under pressure and the lower part is under tension. The displacement increases with the distance from the failure. In other words, the closer to the failure, the more sensitive the displacement change; the farther away from the damage, the less sensitive the displacement changes. This is due to the phenomenon of stress concentration at the failure site, resulting in a rapid increase in local stress, so its displacement change is more drastic. It is worth explaining that some of the cloud images show that the displacement around it is not

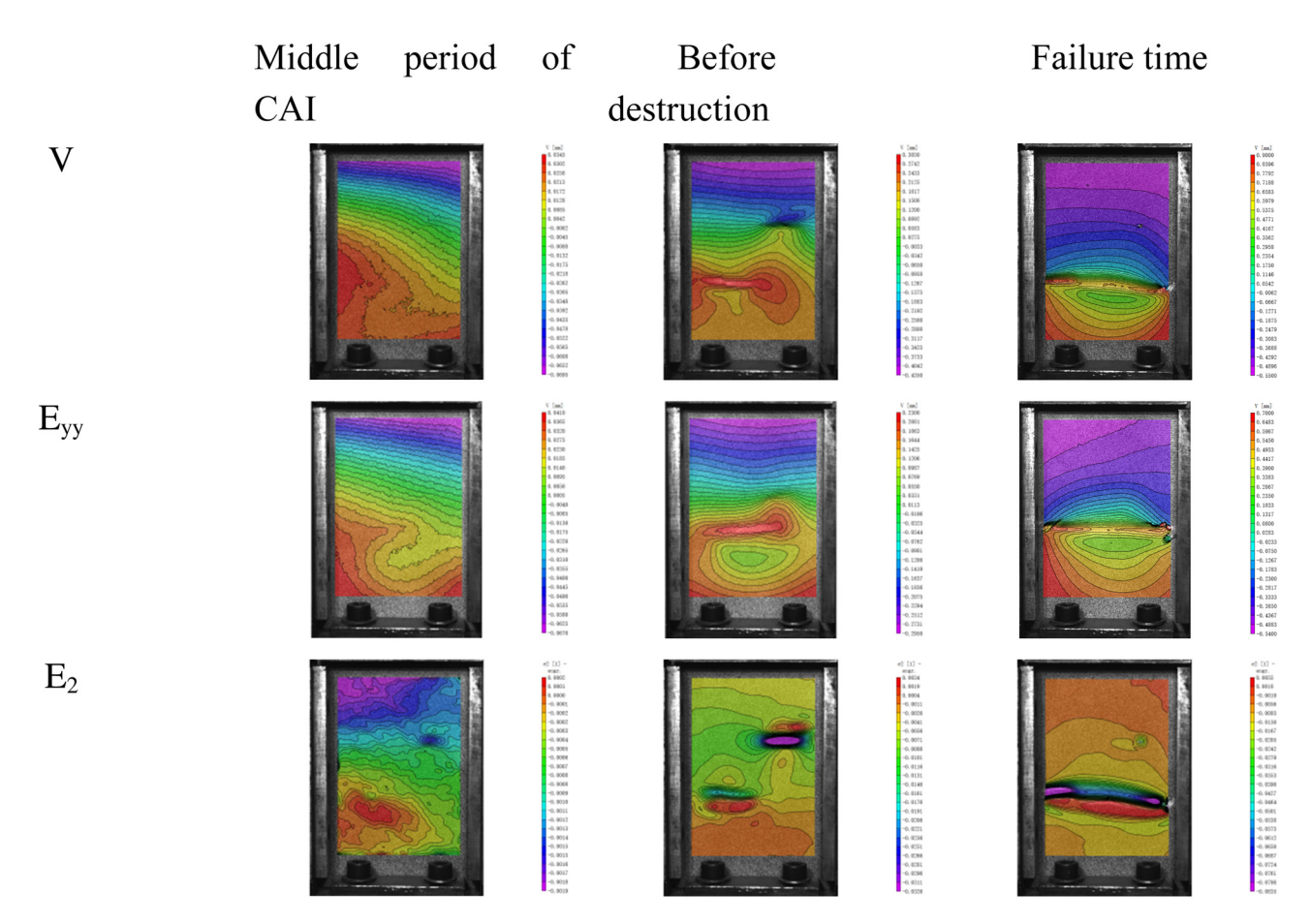


Figure 17: DIC of compression damage in different stages of 25-40J-3.

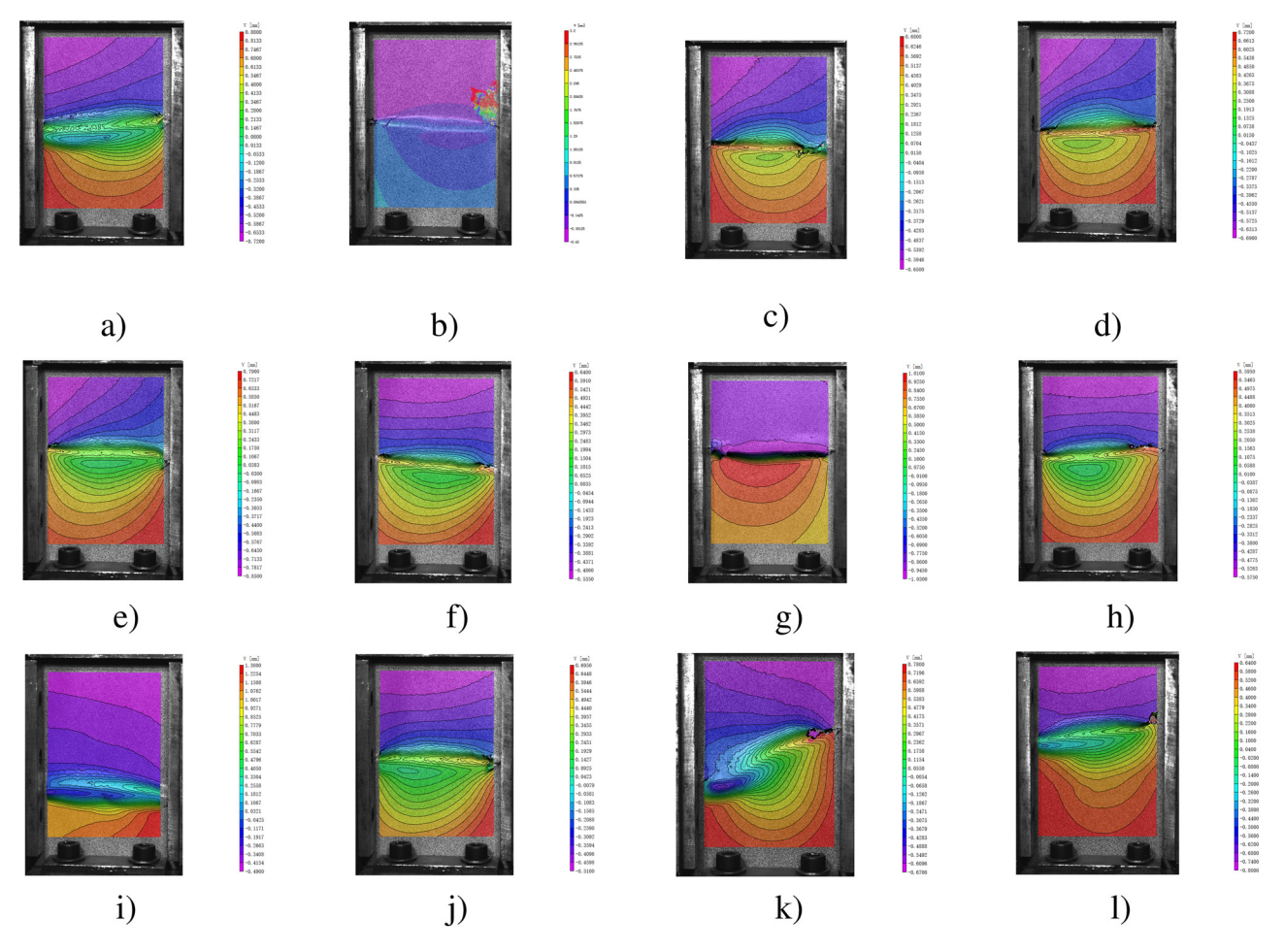


Figure 18: DIC-von mises of 20 J impact energy group compression experiment. (a) 12.5-20J-1, (b) 12.5-20J-2, (C) 12.5-20J-3, (d) 12.5-20J-4, (e) 25-20J-1, (f) 25-20J-2, (g) 25-20J-3, (h) 25-20J-4, (i) 50-20J-1, (j) 50-20J-2, (k) 50-20J-3, and (l) 50-20J-4.

uniform, which is caused by not completely vertical fixation when fixed in the attachment, as shown in Figure 19c and others.

4.3 Damage analysis after compression by C-scan and SEM

The external representation picture of compression failure on the side of the specimen is shown in Figure 21. When the material is impacted, vertical pressure is applied to the center and vicinity of the impact point. Due to the existence of different angles of material layering, shear deformation will also occur between different layering angles, resulting in damage. Under the compression of vertical positive pressure, the failure mainly extends to the impact point and its vicinity. In the process of reaching the ultimate failure load, the installation of the specimen is not completely vertical,

resulting in bending deformation in addition to compression deformation during the compression process. Due to the small transverse moment of inertia, the failure section is extended along the transverse.

Figure 22 shows the SEM image after CAI. From Figure 22, it can be seen that the stripping and failure of the matrix and the fracture of the carbon fiber bundle are relatively obvious. From the analysis of the fracture surface, the main failure is compression and shear. Specific analysis of the reason, laminate materials because of the arrangement of fiber bundles is two-dimensional arrangement, compared with three-dimensional braided materials with stronger integrity, its ability to resist shear failure is lower. Therefore, when the vertical compression test is carried out after the impact damage, the fiber bundles whose alignment angle is inconsistent with the direction of the positive pressure load are more susceptible to shear failure. At the same time, the bonding between the matrix and the matrix mainly depends on the physical high

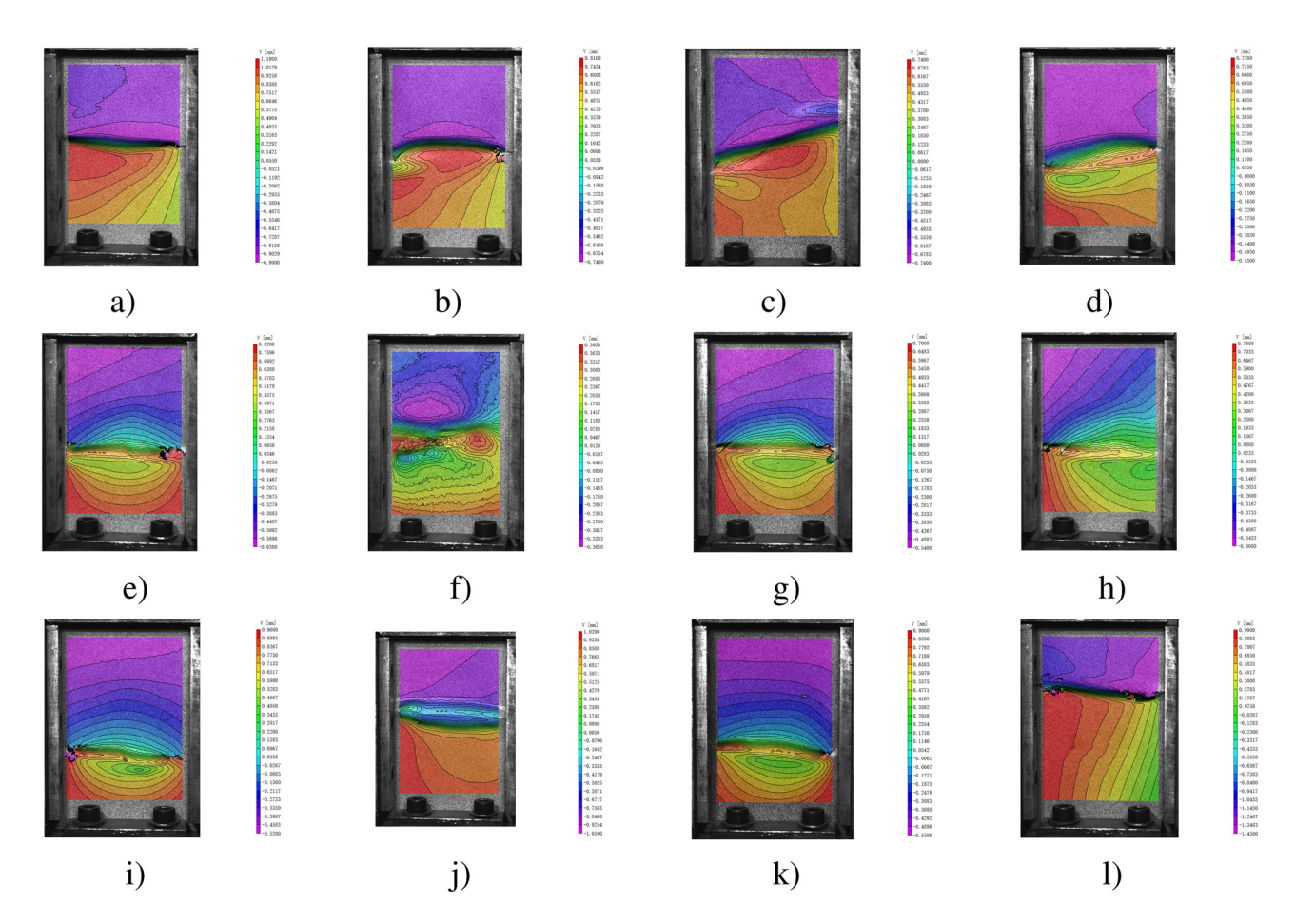


Figure 19: DIC-von Mises of 40J impact energy group compression experiment. (a) 12.5-40J-1, (b) 12.5-40J-2, (C) 12.5-40J-3, (d) 12.5-40J-4, (e) 25-40J-1, (f) 25-40J-2, (g) 25-40J-3, (h) 25-40J-4, (i) 50-40J-1, (j) 50-40J-2, (k) 50-40J-3, and (l) 50-40J-4.

temperature compression, rather than the connection of the structure itself. As a result, its shear strength is also low, so it is seriously affected by shear deformation during compression, and there are often damaged forms of fiber bundle fracture and matrix destruction.

C-scan was also used to scan the specimen, and internal damage areas were obtained. The analysis is as follows.

Figure 23 shows the internal damage diagram of the specimen after compression when the single impact energy is 20 J and the number of impacts is two. The damage location is mainly at the impact location, and the form of failure is penetrating transverse failure, matrix failure and shear failure are the main damage modes, brittle fracture failure is the main failure mode, and the relationship between the damage area and the impact angle of

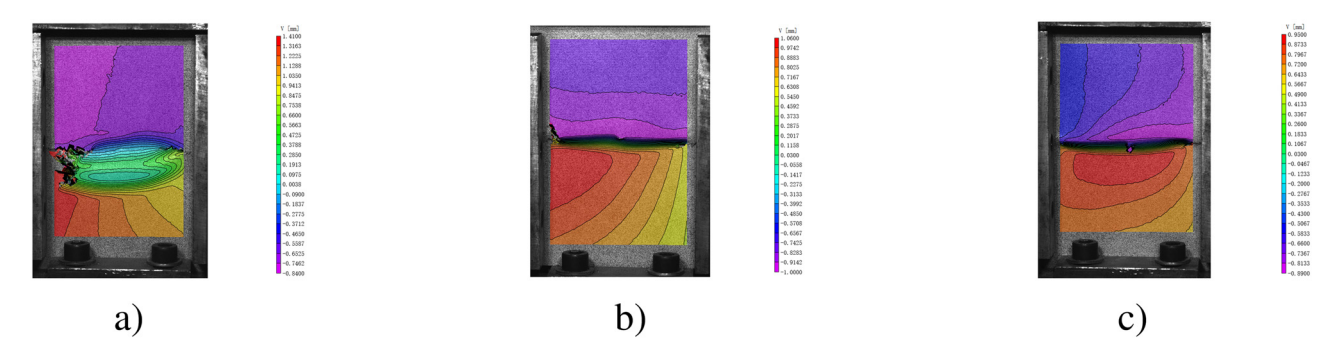


Figure 20: DIC-von Mises of control group compression experiment. (a) 20J-1, (b) 30J-1, and (c) 40J-1.

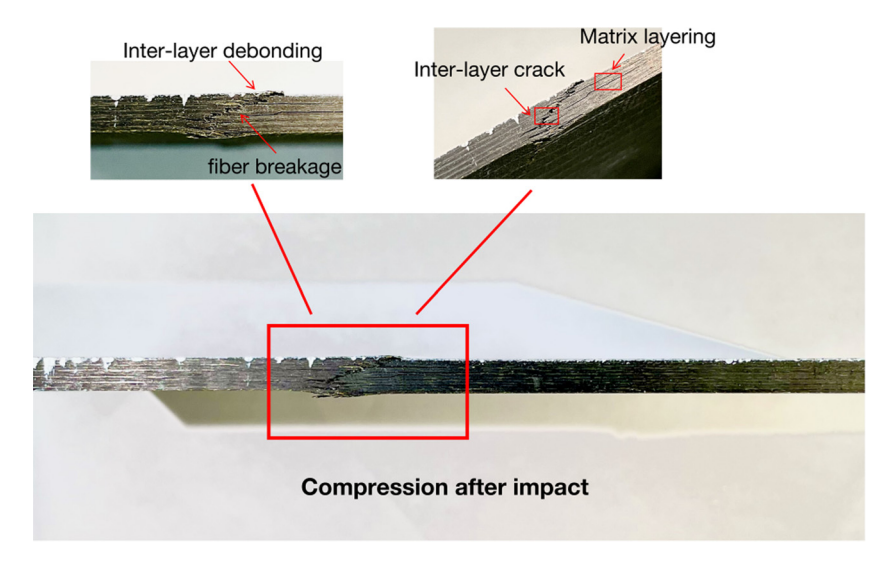


Figure 21: Microscopy images of the cross section of NCF specimen after CAI test.

compression damage is not obvious. In Table 11, the proportion of internal damage of specimens under this group of compression tests is calculated. The size of the damage area has little relationship with the impact angle, and has a positive relationship with the internal damage caused by the impact. This indicates that the larger the area of the original damage area, the greater the damage caused by compression. The comparison of data is shown in Figure 24.

Figure 25 statistically shows the internal damage diagram of the specimen after compression when the single

impact energy is 40 J and the number of impacts is one. It is concluded that the failure form and evolution mode are almost the same as the 20 J impact group. Because the 20 J impact panel is subjected to more shocks, its strength is slightly affected. The internal damage is mainly reflected in the impact distance of 12.5 mm. This is because the smaller the impact distance, the greater the impact coupling effect, resulting in the impact of the number of impacts on the damaged area increased. The proportion of internal damage area after compression of specimens

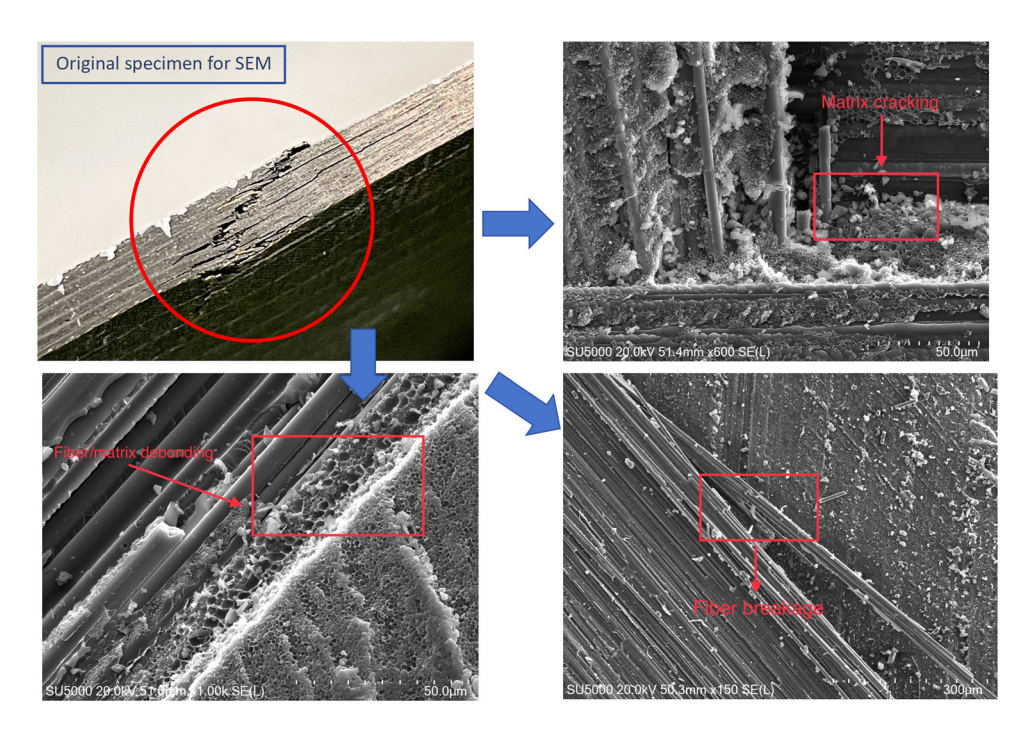


Figure 22: Failure mode under SEM after compression test.

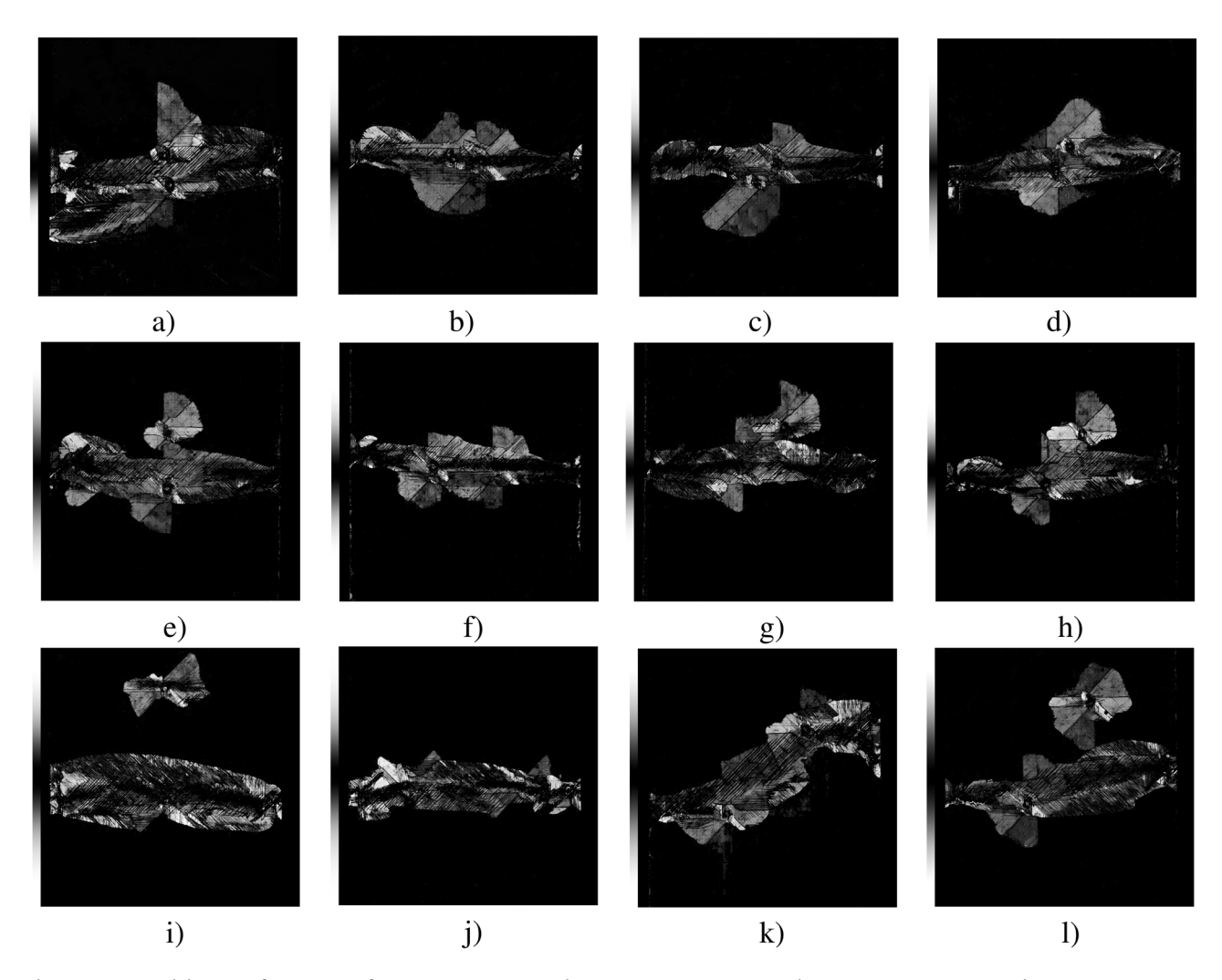


Figure 23: Internal damage of specimens after compression test under 20 J impact. (a) 12.5-20J-1, (b) 12.5-20J-2, (C) 12.5-20J-3, (d) 12.5-20J-4, (e) 25-20J-1, (f) 25-20J-2, (g) 25-20J-3, (h) 25-20J-4, (i) 50-20J-1, (j) 50-20J-2, (k) 50-20J-3, and (l) 50-20J-4.

Table 11: Internal damage proportion of specimens after compression test under 20 J impact

Number	Proportion of damaged areas (%)
12.5-20J-1	27.73
12.5-20J-2	23.65
12.5-20J-3	22.50
12.5-20J-4	23.23
25-20J-1	26.98
25-20J-2	23.86
25-20J-3	25.61
25-20J-4	25.01
50-20J-1	24.73
50-20J-2	21.93
50-20J-3	23.66
50-20J-4	26.34

in the 40 J impact group is shown in Table 12, and the conclusion is the same as above. The relationship between the damage caused by initial impact and the internal damage caused by compression is shown in Figure 26.

The internal damage statistics of the control group are shown in Figure 27. The following conclusions can be drawn: the failure is mainly centered on the impact center, and extends horizontally until the failure occurs, and the failure plane runs through the impact point. The impact position of the control group was located in the geometric center of the plate, and the impact number was single. Therefore, its failure mode under impact and compression is relatively simple. It can be seen from the C-scan figure that the fibers at the impact point are fractured under compression and shear. In the overall vertical compression

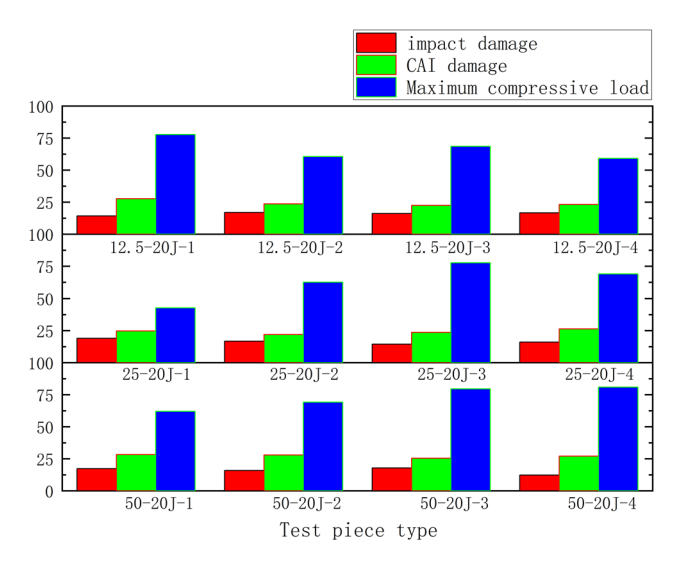


Table 12: Internal damage proportion of specimens after compression test under 40 J impact

Number	Proportion of damaged areas (%)	
12.5-40J-1	25.94	
12.5-40J-2	26.44	
12.5-40J-3	22.90	
12.5-40J-4	21.80	
25-40J-1	28.35	
25-40J-2	27.92	
25-40J-3	25.49	
25-40J-4	27.03	
50-40J-1	25.07	
50-40J-2	25.41	
50-40J-3	26.80	
50-40J-4	24.03	

Figure 24: Comparison of impact damage, CAI damage, and maximum compression load in 20 J.

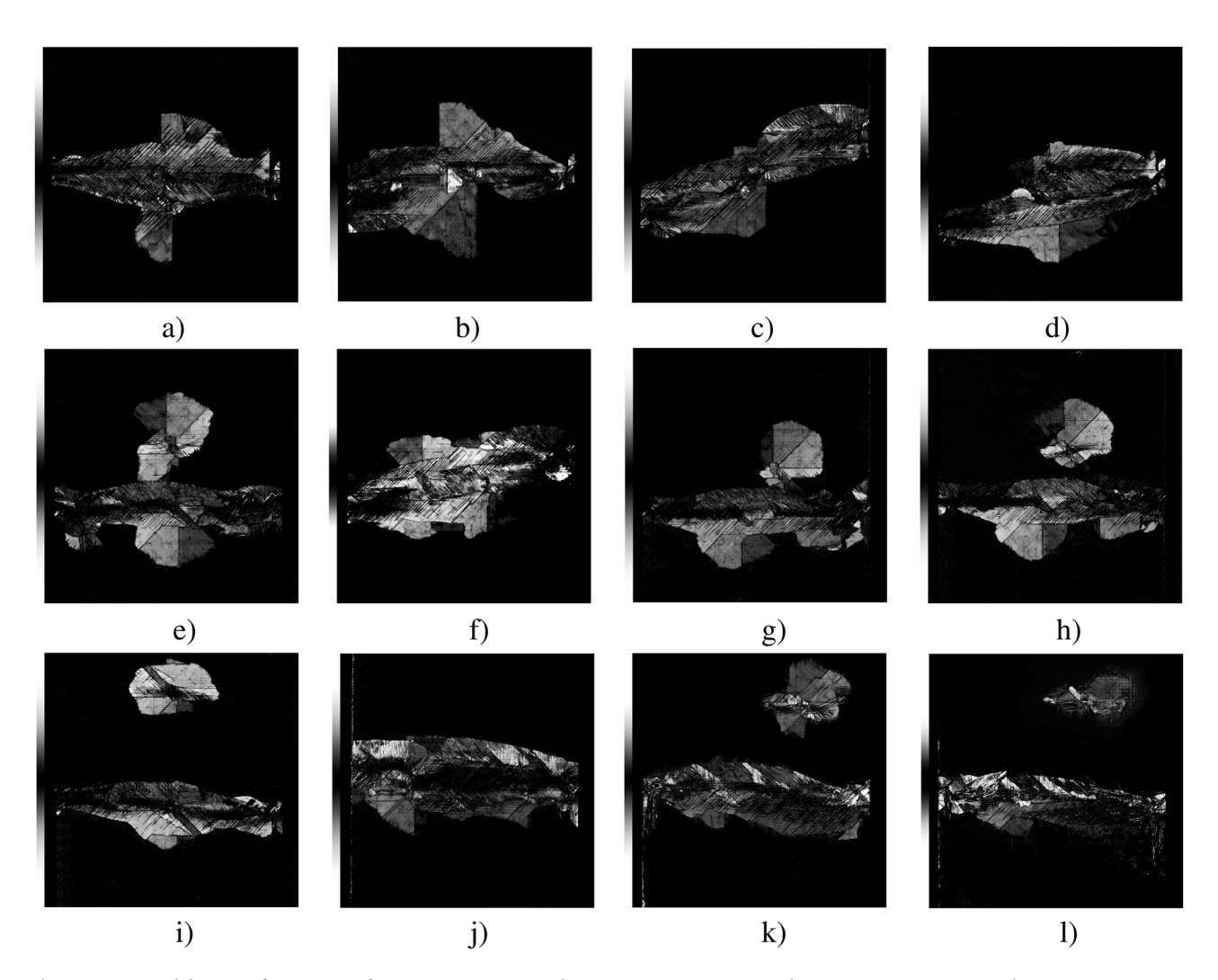


Figure 25: Internal damage of specimens after compression test under 40 J impact. (a) 12.5-40J-1, (b) 12.5-40J-2, (C) 12.5-40J-3, (d) 12.5-40J-4, (e) 25-40J-1, (f) 25-40J-2, (g) 25-40J-3, (h) 25-40J-4, (i) 50-40J-1, (j) 50-40J-3, and (l) 50-40J-4.

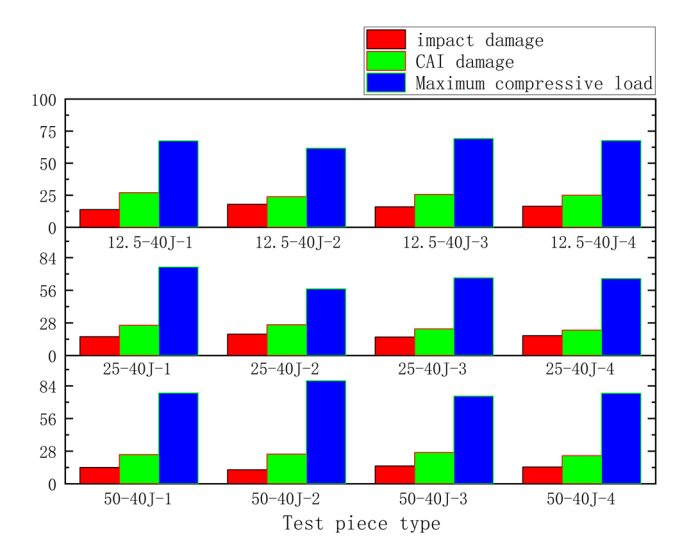


Figure 26: Comparison of impact damage, CAI damage, and maximum compression load in 40 J.

process, penetrating cracks occur along a relatively obvious transverse path until the bearing capacity is completely lost and brittle failure occurs.

The statistics of the internal damage area under the control group test are shown in Table 13, because there is no difference in impact angle in the control group. In the statistical section of the damage area of 30J-1 and 40J-1, the situation is less than the above conclusion. This is because the shadow part in C-scan reflects the sum of all the damaged patterns superimposed from this thickness to the surface layer. Because the thickness selected in the scanning process is not the thickness of the maximum damage, the scanning area is small. In Figure 28, the proportion of internal damage area produced under impact,

Table 13: Internal damage proportion of control group specimens after compression test

Number	Proportion of damaged areas (%)
20J-1	29.11
30J-1	23.10
40J-1	26.23

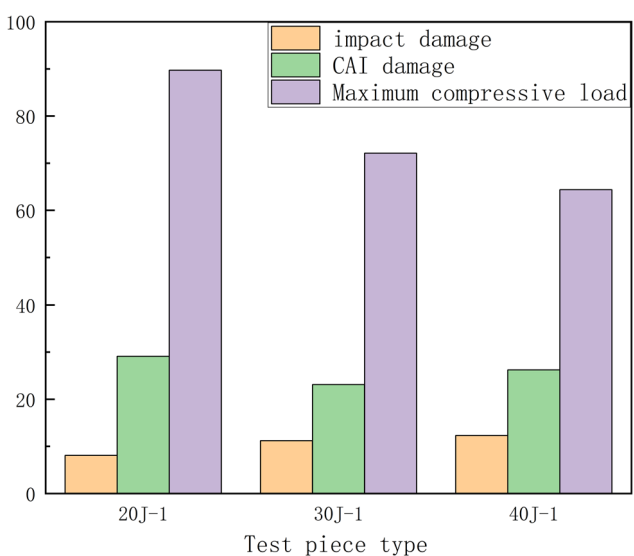


Figure 28: Comparison of impact damage, CAI damage, and maximum compression load in control group.

proportion of damage area produced under compression, and failure load during compression were statistically analyzed, which further confirmed the above views.

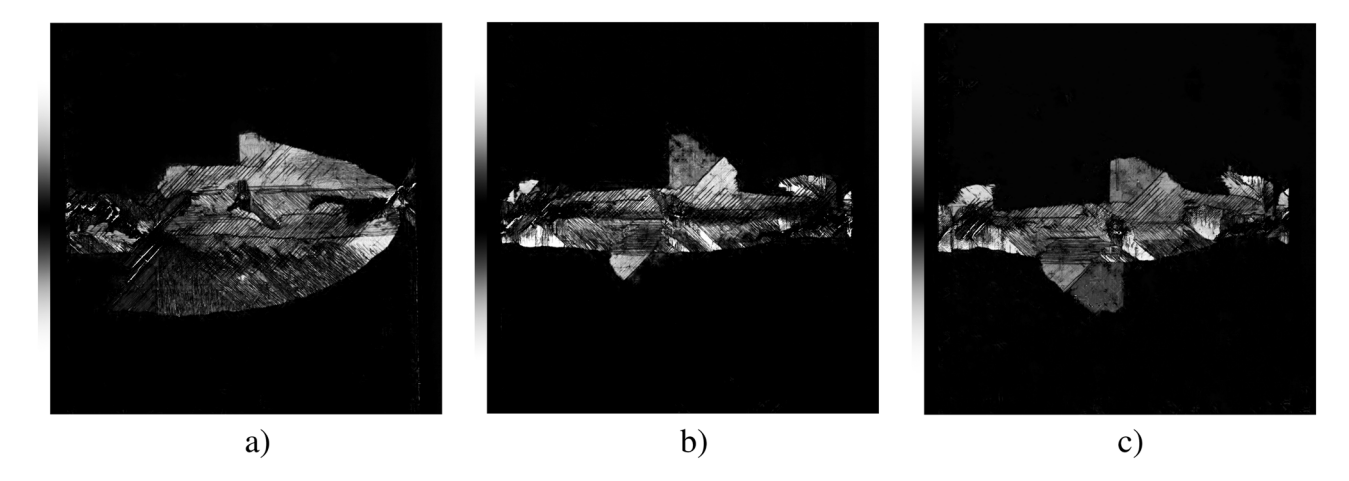


Figure 27: Internal damage of control group specimens after compression test. (a) 20J-1, (b) 30J-1, and (c) 40J-1.

5 Conclusion

5.1 LVI test

The LVI test mainly studied the multiple-impact and singleimpact response and failure process of NCF composites. The experiment was mainly conducted in three groups: under the impact distance of 12.5, 25, and 50 mm, 20 J impact energy was set for single-point, two-time low-speed impact experiment; under the impact distance of 12.5, 25, and 50 mm, 40 J impact energy was set for two-point, single-time low-speed impact experiment; and control group. During the LVI test, the conclusion is as follows:

- 1) With the increase in the number of shocks, the damage generated inside the NCF composite material is further extended, resulting in the strength of the material decreasing with the increase in the number of shocks;
- 2) The increase in impact distance will lead to coupling impact effect, making the two impact tests more independent;
- 3) Different impact angles have little impact on the impact response, which is reflected in the peak load, stability time, time-load curve, internal damage, etc., which are almost the same:
- 4) The ultimate load generated under 40 I impact is almost twice as high as the ultimate load generated under 20 J impact. This indicates that there is a linear increasing relationship between the ultimate bearing capacity and the impact energy before the specimen is completely crushed and loses its strength
- 5) After the impact, the upper surface of the specimen showed a depression, and the fibers in the depression were mainly compressed and bent. However, there were no obvious cracks and fiber fracture traces, and fiber bundle fractures along the 45° layup direction on the lower surface, and slight fault signs began to appear. The impact failure extension direction is consistent with the fiber layering direction of the failure layer, which has strong directivity.
- 6) When the impact distance is 12.5 mm, internal damage occurs during the impact process (mainly layered damage). After multiple shocks, the strength of the material is reduced, and the failure direction is not significant due to the impact coupling effect.

5.2 CAI test

According to the results of displacement - load curves, Cscan and SEM, CAI test mainly discusses the influence of LVI test on load limit and compressive properties of specimens. Through direct observation and NDT technology (Cscan, SEM) to explore its failure mode, the conclusion is as follows:

- 1) In the failure process, the main failure forms are matrix fracture and fiber fracture. The main damage failure form is shear failure. The main failure mode is brittle fracture. The main failure position appears at the impact position, which is manifested in the form of penetrating lateral failure. The maximum stress occurs at the failure layer, and the impact angle has little effect on the fracture direction. The oblique fracture occurs only when the oblique is 45° and the impact distance is large (50 mm). During the failure, the overall failure tendency is divided into upper compression and lower tension. The displacement increases with the distance from the failure place, that is, the closer to the failure place, the more sensitive the displacement change. The farther away the damage place is, the less sensitive the displacement change is.
- 2) The area of the damaged area has little relationship with the angle of impact, but it is proportional to the internal damage caused by impact, that is, the larger the area of the original damaged area, the greater the damage caused by compression;
- The greater the number of shocks, the greater the decline in strength, and the greater the internal damage area caused by external loads.

Funding information: This research was funded by the National Natural Science Foundation of China [No. 11972140], National Natural Science Foundation of China [No. 12002003]. Natural Science Foundation of Hebei Province [No. A2023409007] and Xiamen city university high-level talent research startup funding project (G1L2023-2) are acknowledged for supporting this research.

Author contributions: Conceptualization: Shi Yan and Lili Jiang; methodology: Shi Yan; writing - original draft preparation: Yuxuan Zhang; supervision: Shi Yan; collating: Tiancong Fan; article proofreading: Junjun Zhai; material supply and testing: Hanhua Li. All authors have accepted responsibility for the entire content of this manuscript and approved its submission.

Conflict of interest: The authors state no conflict of interest.

Data availability statement: The datasets generated during and/or analysed during the current study are available from the corresponding author on reasonable request.

References

- Paredes-Gordillo, M. A., I. Iváñez, and S. K. García-Castillo. Numerical study of the simultaneous multiple impact phenomenon on CFRP plates. Composite Structures, 2023, p. 117194.
- Xu, Y. M., P. Z. Zhu, and W. Z. Wang. Study of multiple impact behaviors of CFRP based on peridynamics. Composite Structures, Vol. 322, 2023, p. 117380.
- García-Rodríguez, S. M., J. Costa, A. Bardera, V. Singery, and D. Trias. A 3D tomographic investigation to elucidate the lowvelocity impact resistance, tolerance and damage sequence of thin non-crimp fabric laminates: Effect of ply-thickness. Composites Part A: Applied Science and Manufacturing, Vol. 113, 2018, pp. 53-65.
- Bibo, G. A., P. J. Hogg, and M. Kemp. Mechanical characterisation of glass- and carbon-fibre-reinforced composites made with noncrimp fabrics. Composites Science and Technology, Vol. 57, No. 9-10, 1997, pp. 1221-1241.
- [5] Falcó, O., C. S. Lopes, D. E. Sommer, D. Thomson, R. L. Ávila, and B. H. A. H. Tijs. Experimental analysis and simulation of low-velocity impact damage of composite laminates. Composite Structures, Vol. 287, 2022, p. 115278.
- Agir, I., A. Kursun, and N. B. Bektas. Investigation of experimental research on the low velocity impact damage behavior of Ncf composite plates - COMPLAS XII. COMPLAS XII: proceedings of the XII International Conference on Computational Plasticity: fundamentals and applications, COMPLAS XII: proceedings of the XII International Conference on Computational Plasticity: fundamentals and applications, 2013.
- Atas, C., Y. Akgun, O. Dagdelen, B. M. Icten, and M. Sarikanat. An experimental investigation on the low velocity impact response of composite plates repaired by VARIM and hand lay-up processes. Composite Structures, Vol. 93, No. 3, 2011, pp. 1178-1186.
- [8] Shyr, T.-W. and Y.-H. Pan. Impact resistance and damage characteristics of composite laminates. Composite Structures, Vol. 62, 2003,
- Shyr, T.-W. and Y.-H. Pan. Low velocity impact responses of hollow core sandwich laminate and interply hybrid laminate. Composite Structures, Vol. 64, No. 2, 2004, pp. 189-198.
- [10] Saito, H. and I. Kimpara. Evaluation of impact damage mechanism of multi-axial stitched CFRP laminate. Composites Part A: Applied Science and Manufacturing, Vol. 37, No. 12, 2006, pp. 2226-2235.
- [11] Bouvet, C., S. Rivallant, and J. J. Barrau. Low velocity impact modeling in composite laminates capturing permanent indentation. Composites Science and Technology, Vol. 72, No. 16, 2012, pp.
- [12] Shi, Y., T. Swait, and C. Soutis. Modelling damage evolution in composite laminates subjected to low velocity impact. Composite Structures, Vol. 94, No. 9, 2012, pp. 2902-2913.
- [13] Hongkarnjanakul, N., C. Bouvet, and S. Rivallant. Validation of low velocity impact modelling on different stacking sequences of CFRP laminates and influence of fibre failure. Composite Structures, Vol. 106, 2013, pp. 549-559.
- [14] Furtado, C., A. Arteiro, G. Catalanotti, J. Xavier, and P. P. Camanho. Selective ply-level hybridisation for improved notched response of composite laminates. Composite Structures, Vol. 145, 2016, pp. 1–14.

- [15] Arteiro, A., G. Catalanotti, J. Xavier, and P. P. Camanho. Large damage capability of non-crimp fabric thin-ply laminates. Composites Part A: Applied Science and Manufacturing, Vol. 63, 2014, pp. 110-122.
- [16] Arteiro, A., G. Catalanotti, J. Xavier, P. Linde, and P. P. Camanho. A strategy to improve the structural performance of non-crimp fabric thin-ply laminates. Composite Structures, Vol. 188, 2018, nn. 438-449.
- [17] Sasikumar, A., D. Trias, J. Costa, N. Blanco, J. Orr, and P. Linde. Impact and compression after impact response in thin laminates of spread-tow woven and non-crimp fabrics. Composite Structures, Vol. 215, 2019, pp. 432-445.
- [18] Syed Abdullah, S. I. B., L. Iannucci, E. S. Greenhalgh, and Z. Ahmad. The impact performance of vectran/epoxy composite laminates with a novel non-crimp fabric architecture. Composite Structures, Vol. 265, 2021, p. 113784.
- [19] Nesbitt, S. The Effect of Impactor Mass and Velocity on the Structural Response and Damage Modes of Non-Crimp and 2D Braided CFRP Panels, University of British Columbia, 2020.
- [20] Vallons, K., A. Behaeghe, S. V. Lomov, and I. Verpoest. Impact and post-impact properties of a carbon fibre non-crimp fabric and a twill weave composite. Composites Part A: Applied Science and Manufacturing, Vol. 41, No. 8, 2010, pp. 1019-1026.
- [21] Gouskos, D. and L. Iannucci. A failure model for the analysis of cross-ply Non-Crimp Fabric (NCF) composites under in-plane loading: Experimental & numerical study. Engineering Fracture Mechanics, Vol. 271, 2022, p. 108575.
- [22] Saeedifar, M., M. N. Saleh, H. M. El-Dessouky, S. Teixeira De Freitas, and D. Zarouchas. Damage assessment of NCF, 2D and 3D woven composites under compression after multiple-impact using acoustic emission. Composites Part A: Applied Science and Manufacturing, Vol. 132, 2020, p. 105833.
- [23] Saleh, M. N., H. M. El-Dessouky, M. Saeedifar, S. T. De Freitas, R. J. Scaife, and D. Zarouchas. Compression after multiple low velocity impacts of NCF, 2D and 3D woven composites. Composites Part A: Applied Science and Manufacturing, Vol. 125, 2019, p. 105576.
- [24] Argon, A. S. Fracture of composites. *Treatise on Materials Science and* Technology, Vol. 1, 1972, pp. 79-114.
- [25] Shipsha, A., M. Burman, and J. Ekh. Failure of cross-Ply NCF composites under off-axis compressive loads - an experimental study and a new strength prediction model including fibre bundle waviness. Composites Part B: Engineering, Vol. 153, 2018, pp. 49-56.
- [26] Seyyednourani, M., S. Akgun, H. Ulus, M. Yildiz, and H. S. Sas. Experimental investigation on compression-after-impact (CAI) response of aerospace grade thermoset composites under lowtemperature conditions assisted with acoustic emission monitoring. Composite Structures, 2023, p. 117260.
- [27] Al-Nadhari, A., H. Senol, S. Topal, H. Ulus, and M. Yildiz. The Effect of Multiscale Kevlar/Glass Hybridization on the Mechanical Properties and the Damage Evolution of 3D Orthogonal Woven Composites under Flexural and Impact Loadings. Composites Part A: Applied Science and Manufacturing, Vol. 175, 2023, p. 107753.
- Wang, B., S. Ci, C. Di, J. Yu, B. Zhu, and K. Qiao. Effects of hygro-[28] thermal and salt mist ageing on the properties of epoxy resins and their composites. Polymers, Vol. 15, 2022, p. 725.